Modelling high temperature effects on bridge slabs reinforced with GFRP rebars

Roberto Pagani, Massimiliano Bocciarelli, Valter Carvelli *, Marco Andrea Pisani

Department of Architecture, Built Environment and Construction Engineering, Politecnico di Milano, Piazza Leonardo da Vinci 32, 20133 Milan, Italy

Article history:
Received 8 June 2014
Revised 12 September 2014
Accepted 6 October 2014

1. Introduction

A major maintenance expense for many transportation departments placed in cold areas is the replacement of bridge slabs to repair corrosion induced deterioration. "Chloride-ion-induced corrosion damage of reinforced concrete bridges is the single most costly deterioration mechanism facing state highway agencies in the United States" (see [1]). It is estimated that about 40% of the current backlog of bridge repairs are a direct result of chloride-ion-induced corrosion of steel reinforcement [1], primarily brought about by the de-icing salts spread on the riding surface of the bridge deck to melt ice during winter months.

Corrosion protection can be pursued by means of reinforcement coatings, migrating corrosion inhibitors, or cathodic protection. The most common and cost effective solution is the use of coated steel reinforcement such as epoxy coated steel rebars or galvanized rebars. However experience has shown that these coatings cannot completely prevent deterioration [2,3].

Another potential solution to guarantee durability of the reinforcement is the use of expensive stainless steel rebars, or much cheaper glass fibre reinforced polymer (GFRP) rebars.

In addition to being corrosion resistant GFRP rebars have a good behavior at low temperatures (that is at least up to −50 °C, see [4–6]) and under cyclic loading (see [7,8]), low thermal conductivity, high strength and low weight (easy placement).

Starting from 1990 GFRP rebars have been used in bridge decks placed in very severe environmental conditions, mainly in Canada (see [9,10]). Nevertheless, many questions related to the adoption of this composite material still need to be investigated in more depth, see [11]. In particular, GFRP presents poor resistance to elevated temperature due to the low value of the glass transition temperature of the polymeric matrix that can be even close to 80 °C. A temperature of this level is higher than the thermal loads due to seasonal changes and solar radiation in bridge decks [12,13], but could be easily overcome during fire exposure.

A bridge deck may be interested by different types of fire. A vehicle burning on a bridge deck cannot damage the GFRP rebars because they are under the source of heating, and are protected by asphalt concrete and concrete cover.

The case of fire under the bridge is much more dangerous both for strength and durability of the bridge deck. A distinction is needed in this case: when dealing with maximum temperatures higher than 600 °C the real problem is the rapid strength decrease of the structure, independently of the type of rebar adopted (see for instance [14–17]). On the contrary, when the maximum sustained temperature does not exceed approximately 600 °C concrete strength does not tremendously decrease, see [18,19], whereas bond between GFRP rebars and concrete vanishes.

Temperatures higher than 600 °C can be reached only in particular extremely rare conditions, e.g. a truck carrying inflammable substances burning under a flyover, whereas a bushfire should not heat the bridge deck over 550 °C, at least according to simulations made by some of the authors with the open source software

* Corresponding author. Tel.: +39 02 2399 4354.
E-mail address: valter.carvelli@polimi.it (V. Carvelli).

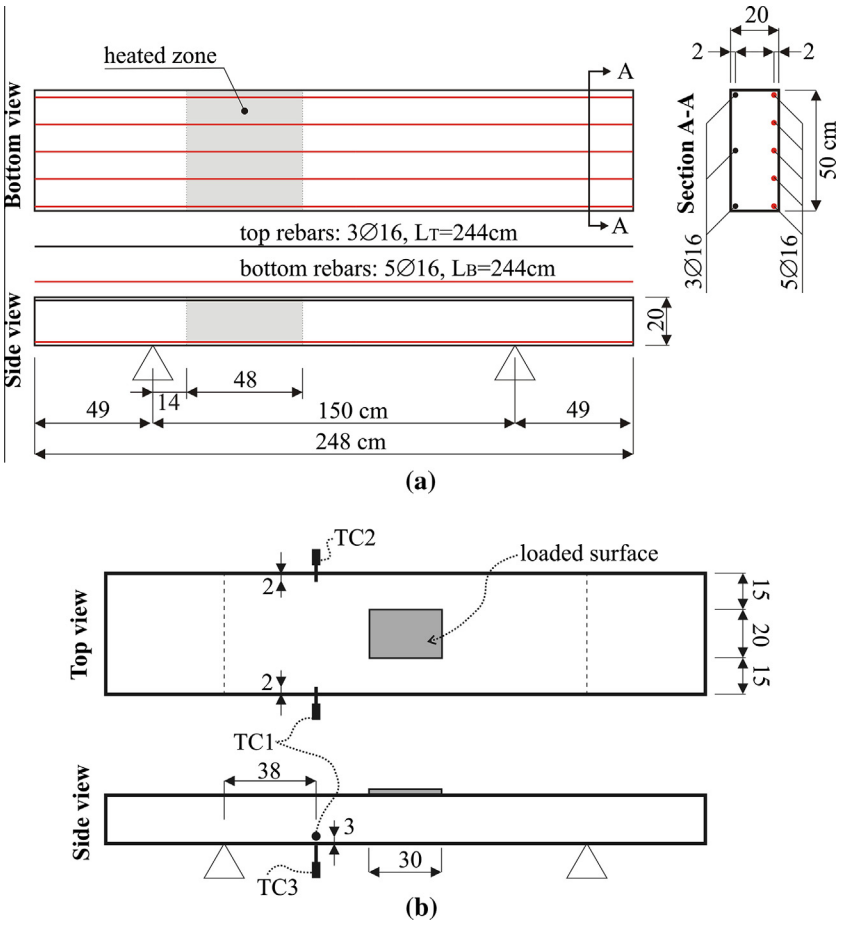

Fig. 1. (a) Geometry and reinforcement of the specimen; (b) thermocouples (TC) position.

'Fire Dynamics Simulator', see [20]. In fact, if the height of a bridge deck is not greater than 10 m, the vegetation cannot grow and thicken too much under it, whereas when dealing with a much higher bridge deck (not less than 20 m) the trees can grow under it and therefore make up a bushfire, but the flames will nevertheless be in open air and far from the deck.

In a previous paper [21] a series of specimens (0.5 m wide, 2.5 m long and 0.2 m thick) were tested both at room temperature and after heating up to 550 °C. These beams correspond to a strip, orthogonal to the bridge beams axis, of full scale bridge slab prototypes (2.5 m wide, 5.0 m long and 0.2 m thick) reinforced with 16 mm diameter GFRP rebars previously tested under monotonic and cyclic loading [7]. The design of these elements was based on the European codes [22–24] to define both the acting loads and the mechanical properties of concrete.

The aims of this paper are: to estimate the ability of bridge slabs reinforced with GFRP rebars to resist to a bushfire, to assess the reduction of efficiency of the slab related to this accidental event and, last but not least, to suggest design details suitable for mitigating the vulnerability of the rebars. The spirit is that of a designer, who does not need very sophisticated numerical models but rather a group of approximate but plausible analyses that can enable him to guarantee the reliability of the structure under this event, or to improve the project when needed. This goal is pursued with analytical and FEM simulations made on a strip representative of the bridge slab both in terms of global deformation and of failure mode. The accuracy of the predictions is assessed by means of comparisons with some of the experimental results available in [21].

2. Overview of the experimental investigation

The experimental tests adopted to validate the analytical and FEM simulations are described in [21]. They deal with narrow strips of a bridge slab reinforced with four different schemes of GFRP rebars. The main interest of the original paper was to study the efficiency of GFRP rebars overlapping in a bridge slab after heating, and to suggest effective solutions.

In this paper the reinforcement scheme with continuous rebars is considered (no overlapping, see Fig. 1a) and tests made both at room temperature and at 550 °C are used.

The unidirectional E-glass fibre reinforced/vynilester (GFRP) bars have a nominal diameter of 16 mm. The external surface of the rebars has a spiral wound yarn along the length and quartz sand to increase bond to concrete. The mechanical properties of the rebars were experimentally measured and detailed in [25]. At room temperature, the GFRP bars have longitudinal tensile strength of 885 MPa and tensile modulus of 39 GPa.

The mechanical properties of concrete at room temperature are: cylindrical compression strength of 49.8 MPa; tensile strength of 4 MPa measured by indirect tensile tests (see the standard EN 12390-6). The degradation of the mechanical properties after heating for 2 h at 550 °C was measured in [21]. The cylindrical compression strength decreased to 23.3 MPa, while the residual tensile strength was 1.1 MPa.

Temperature increase (when acting) was imposed on a portion of the bottom surface of 48 × 50 cm (see grey shaded rectangles in Fig. 1) of the unloaded specimen. The temperature was continuously recorded during heating in three different positions of the

heated zone (see Fig. 1b): in the center of the heated area and in the mid-span on both longitudinal edge sides located 3 cm from the bottom and 2 cm inside the concrete to monitor the temperature close to the GFRP rebars [21].

The maximum temperature recorded close the bottom GFRP rebars was ≈400 °C. This temperature allows neglecting the expansion of the quartz sand consequence of the reversible change in crystal structure of the quartz (from α- to β-quartz). The α- to β-quartz inversion appears above 573 °C.

The specimen still hot was then subjected to a quasi-static loading with a contact surface of 30 × 20 cm, similarly to what previously done for other tests on bridge slabs under monotonic and cyclic loading [7].

3. Analytical model

The proposed analytical formulation, modelling the thermo-mechanical behavior of a concrete strip reinforced with GFRP bars, is based on the following assumptions:

- linear elastic behavior of GFRP and elasto-"plastic" for concrete;
- planarity of the cross-section after bending throughout fire exposure;
- perfect bond between concrete and GFRP rebars. It is a matter of fact that deterioration of the mechanical properties of GFRP (especially strength and Young's modulus), as well as the bond properties, starts when temperature reaches values close to the glass transition temperature [26], that is between 70 °C and 180 °C depending on the type of resin. Nevertheless, both decrease of Young's modulus and bond properties of the rebars will be globally taken into account by means of a reduction of Young's modulus, consistently to the simplified method suggested in [27].

The analytical model is summarized describing: the constitutive laws adopted and the dependency of the materials parameters on the temperature, the moment-curvature curves and, finally, the load–displacement relationship.

3.1. Materials constitutive behavior

When dealing with thermo-mechanical problems, the total strain $\varepsilon^{tot}_{c(g)}$ in both concrete (c) and GFRP rebar (g) is computed as the sum of the elastic (i.e. mechanical) $\varepsilon^{el}_{c(g)}$ and thermal component $\varepsilon^{th}_{c(g)}(T)$, as follows:

$$\varepsilon^{tot}_{c(g)} = \varepsilon^{el}_{c(g)} + \varepsilon^{th}_{c(g)}(T) \tag{1}$$

being the thermal deformation developed in concrete and GFRP rebars, function of the temperature T according to the following relationships:

$$\varepsilon^{th}_{c}(T) = \begin{cases} -1.8\cdot10^{-4} + 9\cdot10^{-6}\cdot T + 2.3\cdot10^{-11}\cdot T^3 & \text{if } 20\,^\circ\text{C} \leqslant T \leqslant 700\,^\circ\text{C} \\ 14\cdot10^{-3} & \text{if } 700\,^\circ\text{C} \leqslant T \leqslant 1200\,^\circ\text{C} \end{cases} \tag{2}$$

$$\varepsilon^{th}_{g}(T) = 6.58\cdot10^{-6}\cdot(T - 20\,^\circ\text{C}) \tag{3}$$

Eq. (2) is suggested in [28]; while Eq. (3) assumes the classical linear relationship between thermal deformation and temperature (the coefficient of thermal expansion being $6.58\cdot10^{-6}$ as suggested in [29]).

In the material models stress was expressed as function of the mechanical strain component only.

A linear elastic constitutive behavior is assumed for the internal reinforcement as:

$$\sigma_g = E_g(T)\varepsilon^{el}_g \tag{4}$$

being σ_g and ε^{el}_g the GFRP axial stress and elastic strain, respectively and $E_g(T)$ the GFRP temperature dependent Young modulus.

In particular, the decrease of the GFRP elastic modulus at elevated temperatures, due to melting of the polymer matrix, is here taken into account according to the semi-empirical analytical relationships proposed by Nigro et al. [27] and Kodur et al. [30,31]. The former proposed the following non-linear relationship:

$$E_g(T) = \frac{0.28}{0.28 + 6\cdot10^{-12}\cdot T^{4.3}}\cdot E_g(20\,^\circ\text{C}) \tag{5}$$

Being E_g (20 °C) the elastic modulus at room temperature. The latter proposed a relationship distinguishing two ranges of temperatures:

$$E_g(T) = \begin{cases} E_g(20\,^\circ\text{C})\cdot\tanh(-7.91\cdot10^{-3}(T-320.35)+0.525) & \text{if } 0\,^\circ\text{C} \leqslant T \leqslant 400\,^\circ\text{C} \\ E_g(20\,^\circ\text{C})\cdot[0.25 - 4.17\cdot10^{-4}(T-400)] & \text{if } T > 400\,^\circ\text{C} \end{cases} \tag{6}$$

For concrete in compression the stress-strain relationship proposed by Sargin [32], described in Eq. (7), was considered.

$$\sigma_c = -f_c(T)\cdot\frac{-2\frac{\varepsilon^{el}_c}{\varepsilon^{el}_{c2}} + (D-1)\cdot\left(\frac{\varepsilon^{el}_c}{\varepsilon^{el}_{c2}}\right)^2}{1 + D\cdot\left(\frac{\varepsilon^{el}_c}{\varepsilon^{el}_{c2}}\right)^2} \quad \text{if } -\varepsilon^{el}_{cu}(T) \leqslant \varepsilon^{el}_c \leqslant 0 \tag{7}$$

where $\varepsilon^{el}_{c2} = 0.002$ is the mechanical strain corresponding to the concrete compressive strength $f_c(T)$ and $\varepsilon^{el}_{cu}(T)$ is the ultimate mechanical strain. The dependence of these two parameters with the temperature T was defined according to [28]. The material parameter D was assumed equal to $7\cdot10^{-2}\times f_c(T)$.

The behavior of concrete under tensile stress is assumed to be linear elastic up to the tensile strength $f_{ct}(T)$ and then it decreases asymptotically to zero in the softening regime according to the Carreira and Chu relationship [33]:

$$\sigma_c = \frac{\beta\cdot f_{ct}(T)\cdot\left(\frac{\varepsilon^{el}_c}{\varepsilon^{el}_{ct}(T)}\right)}{\beta - 1 + \left(\frac{\varepsilon^{el}_c}{\varepsilon^{el}_{ct}(T)}\right)^{\beta}} \quad \text{if } \varepsilon^{el}_{ct}(T) \leqslant \varepsilon^{el}_c \leqslant 10\cdot\varepsilon^{el}_{ct}(T) \tag{8}$$

where $\varepsilon^{el}_{ct}(T) = f_{ct}(T)/E_c(T)$ represents the tensile mechanical strain at the peak stress $f_{ct}(T)$ and $\beta = 1.5$.

The decrease of concrete tensile strength with temperature is taken into account according to [28]:

$$f_{ct}(T) = \begin{cases} f_{ct}(20\,^\circ\text{C}) & \text{if } 20\,^\circ\text{C} \leqslant T \leqslant 100\,^\circ\text{C} \\ \left(1.0 - \frac{T-100}{500}\right)\cdot f_{ct}(20\,^\circ\text{C}) & \text{if } 100\,^\circ\text{C} \leqslant T \leqslant 600\,^\circ\text{C} \end{cases} \tag{9}$$

At relatively low temperatures, a decrease of E_c is caused by loss of capillary water, while at high temperatures a decrease of E_c is due to the decomposition of individual concrete components (cement paste and aggregate). In the present work, temperature dependent Young's modulus follows the proposal of Stabler [34]:

$$E_c(T) = \begin{cases} (1 - 0.2\cdot(0.01T - 0.2) + 0.01\cdot(0.01T - 0.2)^2)E_c(20\,^\circ\text{C}) & \text{if } 20\,^\circ\text{C} \leqslant T \leqslant 800\,^\circ\text{C} \\ 0 & \text{if } T > 800\,^\circ\text{C} \end{cases} \tag{10}$$

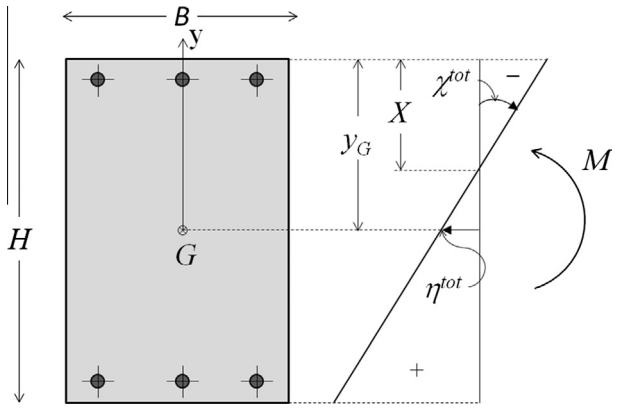

Fig. 2. Geometry of the GFRP reinforced rectangular section; *G* being the center of gravity.

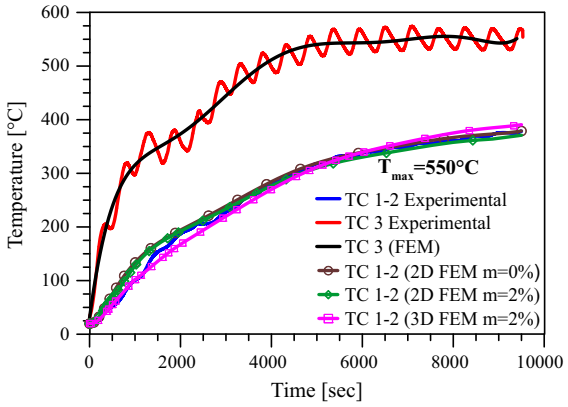

Fig. 4. Temperature histories measured by thermocouples and computed counterparts at different locations of the tested specimens.

3.2. Moment/curvature diagram

According to the above hypotheses, the compatibility equation governing the response of the section can be written as follows, see Fig. 2:

$$\varepsilon^{tot}_{c(g)}(y) = \eta^{tot} - y\chi^{tot} \tag{11}$$

being η^{tot} the total axial strain in the center of gravity of the section (assumed positive in traction) and χ^{tot} the total section curvature.

For a given curvature χ^{tot}, the corresponding moment M can be computed by the following procedure. First the horizontal equilibrium is imposed as:

$$N = \int_A \sigma(\varepsilon^{el}_{c(g)})\,dA \approx \sum_j w_{cj} b_{cj} \sigma_{cj}(\varepsilon^{el}_{cj}) + \sum_i \sigma_{gi}(\varepsilon^{el}_{gi}) A_{gi} = 0 \tag{12}$$

where $\varepsilon^{el}_{c(g)}$ is the mechanical strain computed by means of Eqs. (1) and (11) once the thermal strain $\varepsilon^{th}_{c(g)}(T)$ distribution is known; b_{cj} is the section width in correspondence of each integration point adopted to discretize Eq. (12) along the section; w_{cj} are the weights of the Gaussian integration scheme and A_{gi} is GFRP reinforcement area.

The above equation is non-linear in the unknown η^{tot} and can be solved according to the following iterative Newton–Raphson scheme:

$$\eta^{tot}_{i+1} = \eta^{tot}_i - \left[\sum_j w_{cj} b_{cj} d_{ctj} + \sum_i d_{gtj} A_{gi}\right]^{-1} N_i \tag{13}$$

being d_{ctj} and d_{gtj} the current tangent constitutive modulus of concrete and GFRP, respectively; and N_i the axial stress resultant at the i-*th* iteration.

Once the value of η^{tot} has been computed the strain distribution is known and through the constitutive equations the moment M corresponding to the given curvature χ^{tot} can be derived as:

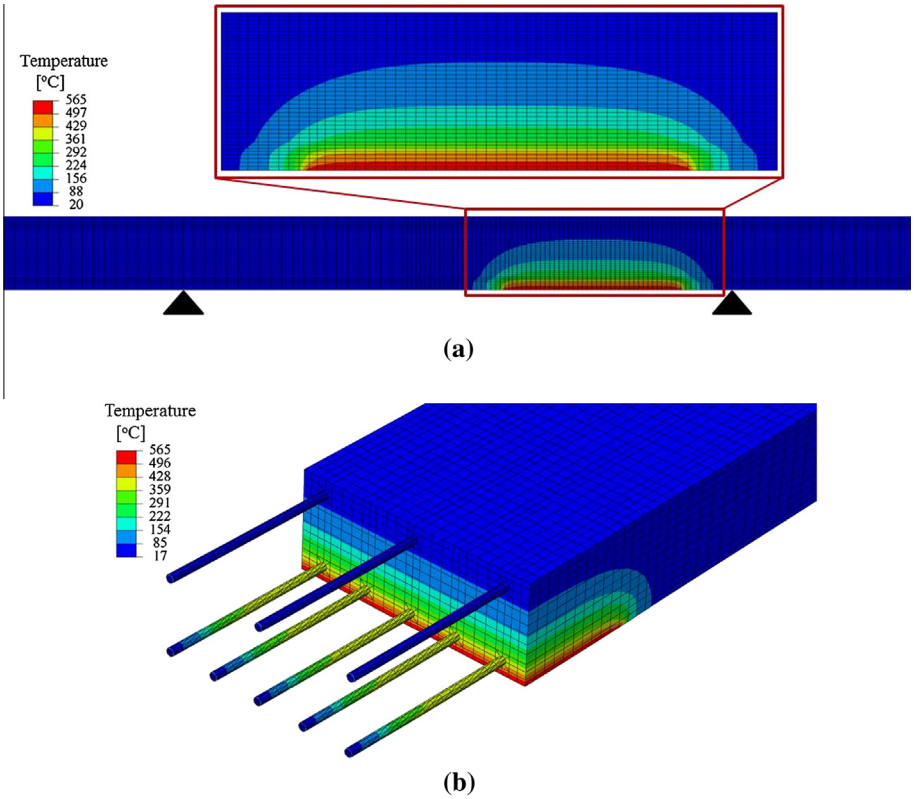

Fig. 3. Temperature distribution at the end of the heating stage computed by (a) 2D plane stress and (b) 3D finite element models.

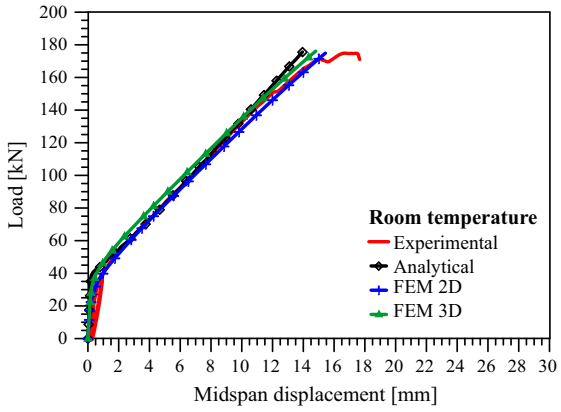

Fig. 5. Load–midspan displacement curves for specimen at room temperature; comparison of experimental, analytical and numerical results.

$$M = -\int_A y\sigma(\varepsilon^{el}_{c(g)})\,dA \approx -\sum_j y_{cj} w_{cj} b_{cj} \sigma_{cj}(\varepsilon^{el}_{cj}) - \sum_i y_{gi}\sigma_{gi}(\varepsilon^{el}_{gi})A_{gi} \qquad (14)$$

Finally the position X of the neutral axis (with respect to the upper part of the section, see Fig. 2) can be computed as:

$$X = y_G - \frac{\eta^{tot}}{\chi^{tot}} \qquad (15)$$

3.3. Load–displacement curve

Once the actual moment distribution M has been computed (by equilibrium equation) and the curvature χ^{tot} derived adopting the corresponding moment–curvature diagram, the displacement, say δ, of a certain section of the reinforced strip can be determined by means of the principle of virtual work:

$$\delta = \int_{beam} M^* \chi^{tot} dx \approx \sum_j w_j M^*_j \chi^{tot}_j \qquad (16)$$

M^* being the bending moment distribution due to a single unit virtual force applied at the specific coordinate where the displacement is determined and w_j the weights of the Gaussian integration scheme adopted to discretize Eq. (16) along the longitudinal direction.

4. Numerical thermo-mechanical models

Two non-linear coupled thermo-mechanical finite element models were developed using the commercial code ABAQUS/Standard [35] to simulate the GFRP reinforced strip bending behavior after local heating, namely plane stress (2D) and three dimensional (3D). For a two-dimensional (2D) model the plane stress assumption seems to be more appropriate than the plane strain considering the geometry of the specimens.

In particular, the temperature distribution after heating, adopted in the analytical model to compute the thermal strain $\varepsilon^{th}_{c(g)}(T)$ through Eqs. (2) and (3), was obtained with the plane stress finite element model.

The 2D FE model adopted reproduces the geometry and loading condition as the specimens tested in the experiments (Fig. 1). The reinforcement was modelled with two strips of height 16 mm and proper width having equivalent area of the GFRP bars. The assumed perfect bond between GFRP bars and the surrounding concrete guarantees the same temperature at the interface.

The initial temperature is set equal to the room temperature. The experimental temperature history was imposed as a prescribed boundary condition on the heated portion of the bottom edge of the model: the temperature increases from 20 to 550 °C in 60 min and then remained constant for 90 min.

The heat transfer problem is nonlinear being the material properties temperature dependent. At elevated temperatures, chemically bounded water on concrete is released gradually as free water and begins to evaporate. During this process, additional heat will be absorbed by the concrete, which affects the temperature development in concrete. Instead of conducting a complex coupled thermo-hydro-mechanical analysis, the concrete specific heat $C_p(T)$ is assumed to be temperature dependent to reflect this influence in the heat transfer analysis, according to [28].

Both concrete density and thermal conductivity were assumed to decrease with temperature according to [28].

GFRP thermal properties were assumed to be constant. In particular the density was taken equal to 1900 kg/m^3, while thermal conductivity was assumed equal to 3.46 W/m °C. Finally, the specific heat was considered to be equal to the one at room temperature, i.e. 1170 J/kg K.

The plane stress finite element model consists of 2268 CPS4T (4-node plane stress thermally coupled quadrilateral) elements, and 7239 degrees of freedom (DOF). The three dimensional finite element model has 31992 C3D8T (8-node thermally coupled brick) elements for the discretization of concrete, and 23178 C3D4T (4-node thermally coupled tetrahedron) elements for the GFRP rebars. The total number of DOFs is 170796. Both models enforce the same constitutive laws and temperature dependent properties described above. To take into account the inelastic behavior of concrete, the concrete damaged "plasticity" model was used. It assumes that the two main failure mechanisms are tensile cracking

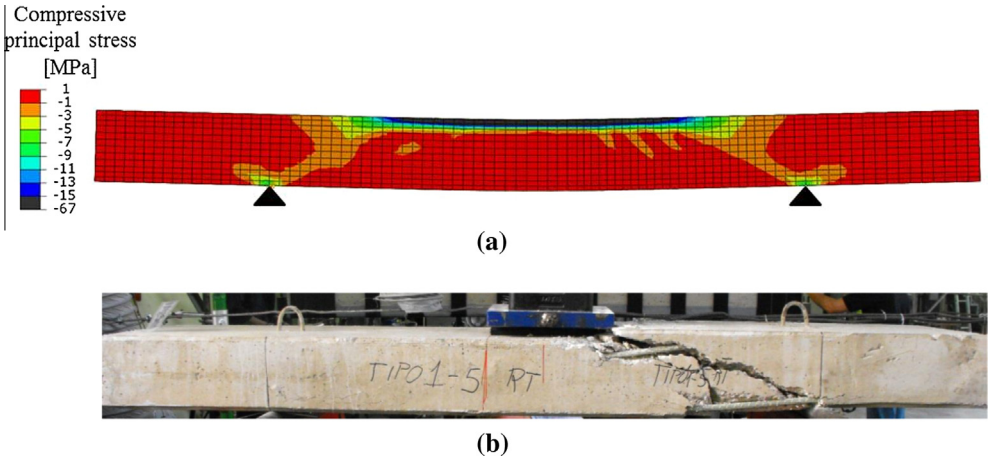

Fig. 6. (a) Numerical compressive principal stress distribution and (b) experimental failure mode of the specimen at room temperature.

and compressive crushing of the material and represents the inelastic behavior of concrete using the yield surface defined by Lubliner et al. [36] and the modifications proposed by Lee and Fenves accounting for different evolutions of strength under tension and compression [37].

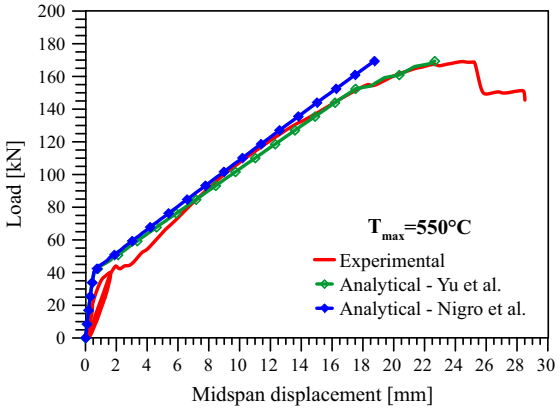

Fig. 7. Load–midspan displacement curves for specimen at elevated temperature (T_{max} = 550 °C); comparison of experimental and analytical results obtained by the analytical procedure proposed in Section 3, endowed with the models in Eqs. (5) and (6).

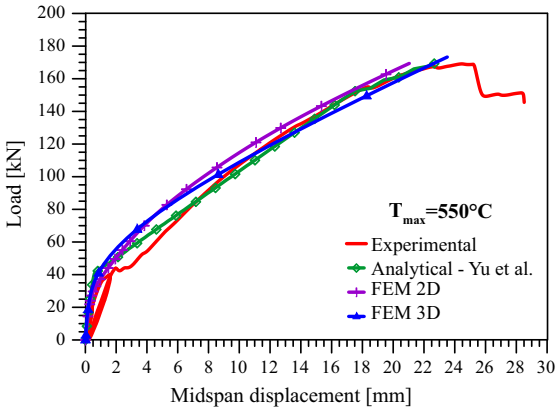

Fig. 8. Load–midspan displacement curves for specimen at elevated temperature (T_{max} = 550 °C); comparison of experimental, analytical (only the model in Eq. (6) proposed in [31] was here considered) and FE models results.

5. Results and comparisons

The two numerical thermo-mechanical models, above described, were used first to define the temperature distribution in the strip. The distribution resulting from the 2D model in Fig. 3 was adopted in the analytical model.

In the experiments the heating source was controlled by a thermocouple placed in the center of the heated zone (thermocouple TC3) while other two thermocouples (TC1 and TC2) were placed inside concrete, see Fig. 1b to monitor continuously the temperature close the GFRP rebars. Fig. 4 shows the temperature histories registered by the thermocouples (TC1-2 represents the mean value of TC1 and TC2 measurements) and the corresponding diagram (TC3 FEM) adopted for FEM analysis. The latter consists in a polynomial fit of the experimental data recorded by thermocouple TC3 (TC3 Experimental) and was applied as a boundary condition (a temperature history, i.e. a thermal load on the heated surface). Moreover, Fig. 4 points out that the thermal response of the model is not significantly influenced by concrete moisture content (m = 0% and m = 2% were analysed). Therefore a standard moisture content of 2% in concrete weight is used in all analyses. The moisture content is taken into account as suggested in [28] through the specific heat.

The mechanical response of the tested strip was compared with the outcomes of the analytical and FEM analyses in terms of load versus midspan displacement at both room temperature and after heating. Fig. 5 compares the results of the analytical model to the experimental and numerical ones (both 2D plane stress and 3D finite element models) at room temperature. Below the cracking load (almost 40 kN) all predictive curves show a slightly higher stiffness with respect to the experimental one. Note that in the experimental tests the specimens were loaded up to cracking and then unloaded, before reloading them up to the ultimate load. Above the cracking load the difference between numerical and experimental values is negligible. However, the predicted ultimate deflection is just slightly smaller than the experimental value. Fig. 6 shows a comparison between the compressive principal stress distribution in the not heated specimen, computed with the 3D FEM model at the experimental ultimate load, and the corresponding experimental failure mechanism. The tied arch mechanism is evident, made of two compressed concrete struts which transmit the applied load to the supports and a tie, i.e. the tension reinforcement. This stress distribution agrees with the collapse mode occurred in the two experimental tests performed, consisting in a shear failure mechanism with a crack between the support and the loading

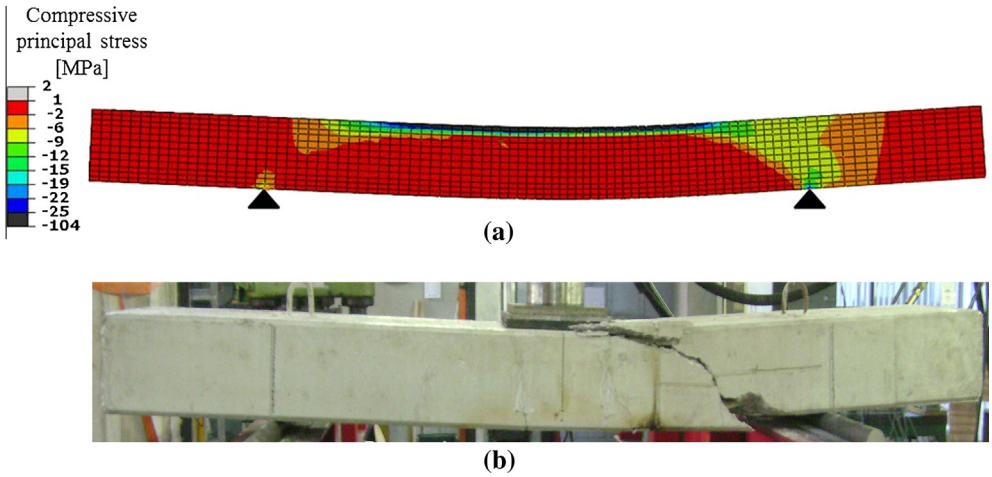

Fig. 9. (a) Numerical compressive principal stress distribution and (b) experimental failure mode of the specimen at elevated temperature (T_{max} = 550 °C).

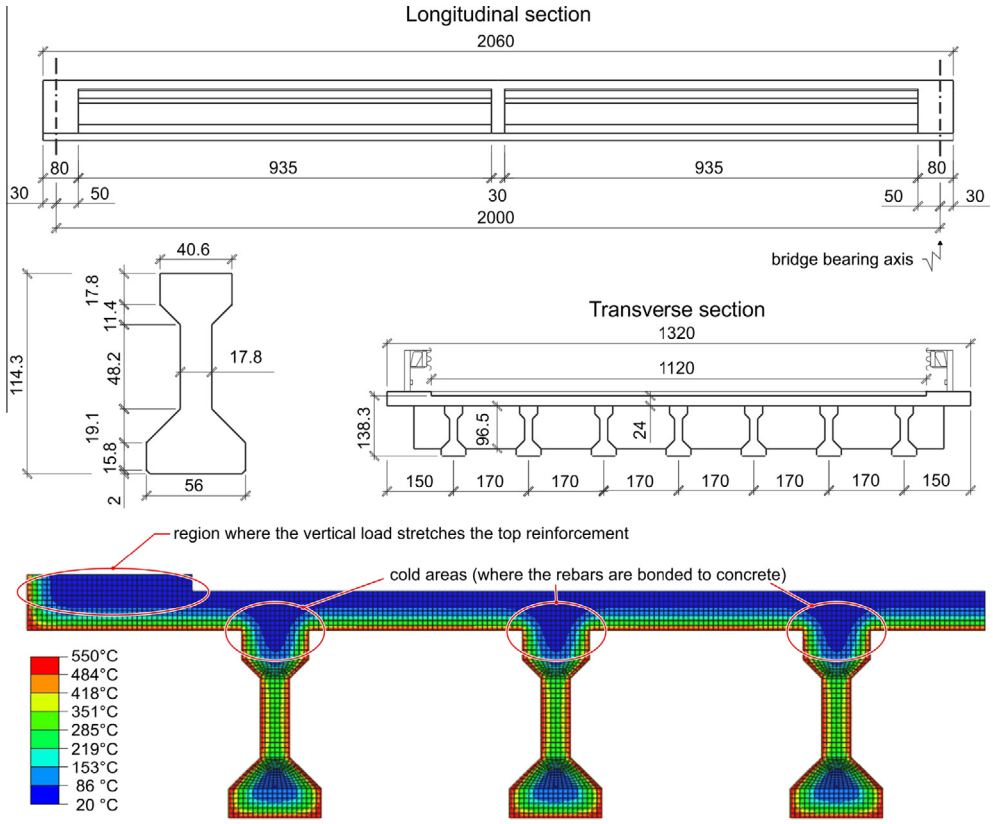

Fig. 10. Bridge deck heating simulation. Temperature distribution at the end of the heating stage computed by finite element model.

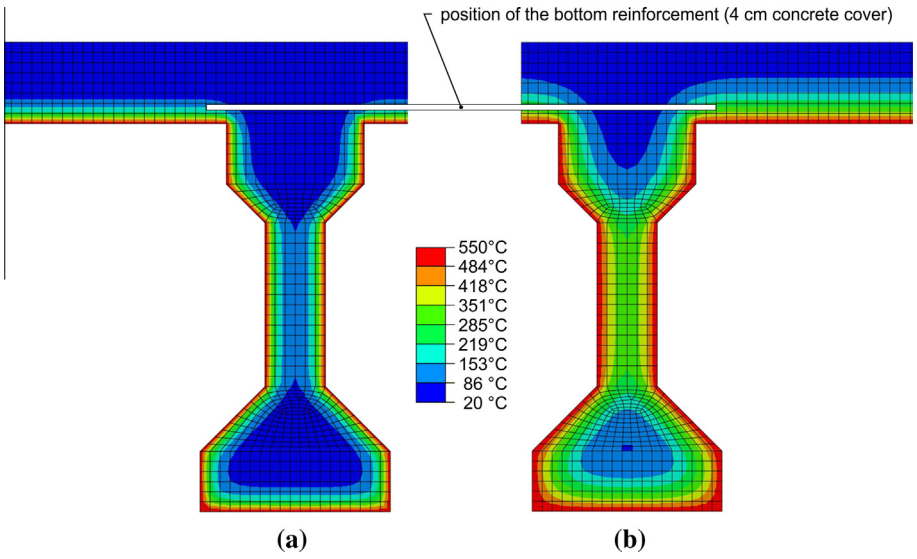

Fig. 11. Bridge deck heating simulation. (a) Temperature distribution after one hour and (b) at the end of the heating stage.

surface. This statement implies that the analytical models cannot determine the load carrying capacity of the structural element, but can nevertheless simulate fairly well its deflection both under service load and when approximating ultimate load, and can be adopted to guarantee low cracking and low vertical displacements when on duty. Note that when dealing with concrete bridge slabs reinforced with GFRP rebars the most unfavourable condition for the bottom reinforcement is not the design load, but the crack width and the deflection (the stiffness) under service loads. This is because strength of a GFRP rebar is usually almost twice that of steel rebar whereas its stiffness is only 1/5.

Fig. 7 depicts the prediction made by the analytical models when the specimen is exposed to the elevated temperature (550 °C). Both the models proposed in [27] and [31], which modify the elastic modulus of the GFRP rebars (see Eqs. (5) and (6) respectively) to take into account the local effects of high temperature (i.e. deterioration of the mechanical and bond properties of FRP) are considered.

Both curves predict correctly the cracking load level, at which a drastic change of stiffness occurs. This phenomenon appears almost at the same load level of the test at room temperature being the heated zone peripheral to the maximum bending moment region.

It is evident that the model proposed in [31] better represents the experimental behavior, particularly at high load levels where increase in the crack opening and consequent slip of the reinforcement occur.

Finally, the results of the 2D and 3D FEM models of the strip exposed to elevated temperature are detailed in Fig. 8 and compared to the experimental and analytical results in terms of load versus midspan displacement. Fig. 8 shows the accurate prediction of the FEM models both at cracking load and at ultimate load, although these models are not able to predict the experimental change of stiffness due to a possible reinforcement slip when approaching the failure load. From this point of view the analytical solution made by means of Eq. (6) looks closer to reality.

Once again in the experimental tests collapse occurred because of shear (see Fig. 9). By comparing Figs. 3, 6 and 9, it looks clear that the failure mechanism does not intersect the heated zone that therefore does not markedly affect the load carrying capacity of the structural element, as shown by the fact that the ultimate load in the two curves is approximately the same.

6. Conclusions

The aim of this paper was to assess the real dangerousness of the event of bushfire on bridge decks reinforced with GFRP rebars by means of analytical and FEM simulations, whose accuracy has been validated by comparisons with some experimental results available in the scientific literature.

The analytical method is able to predict fairly well the evolution of the deflection of the heated bridge slab under service loads and approaching the failure load. It has nevertheless to be pointed out that Eqs. (5) and (6) apply only if the GFRP rebars are well anchored. This can be ensured by avoiding rebars overlapping (i.e. continuous reinforcement should be used in the zone of the concrete element directly exposed to fire) and ensuring a proper anchor length in the cold zones [27,38]. In a stringer bridge the latter condition is usually satisfied:

- in the direction orthogonal to the beams axes because of the local protection exerted by the beams on the bridge slab zone over them (see Fig. 10 dealing with a bridge deck made with AASHTO I beams type III);
- in the direction of travel by anchoring the reinforcement in the end crossbeams.

The fact that in all the experimental tests (see [7,21]) shear failure occurred and that the tensile strength of concrete does not significantly decrease in the core of the slab (because of the low temperature increase, due to the low thermal conductivity of concrete) implies that the load carrying capacity of the bridge deck does not markedly decrease when exposed to relatively high temperatures. On the contrary service problems may arise due to a deterioration of both bond strength and reinforcement Young modulus. The scheme with the bottom reinforcement of the slab unbonded in between the bridge beams is similar to the reinforcement-free bridge decks studied in Canada (see for instance [39]), which, in fact, suffered the problem related to cracking of the bottom surface of the deck slab in the service load range [40]. Similarly, the deterioration of bond strength during heating implies the need to reliably compute the displacements (i.e. the residual stiffness) of the slab under service loads during and after heating. The procedure suggested demonstrated to be reliable. A retrofitting, that is a stiffening of the slab by means of externally bonded CFRP sheets, could then be needed.

A further improvement of the behavior of the bridge deck under bushfire could be achieved by increasing the concrete cover. Last but not least it has to be stated that usually a bushfire does not give rise to a heating that persists for 2.5 h under the slab. Fig. 10 shows that after one hour of heating, according to the curve in Fig. 4, and adopting a 4 cm concrete cover (a finite element in Fig. 11 is 3 cm high) the temperature in the bottom reinforcement is still lower than the glass transition temperature (180 °C) of the adopted polymeric matrix.

In any case the bridge deck could furthermore be protected against bushfire by hanging concrete planks under its bottom.

References

[1] Weyers R, Prowell B, Sprinkel M, Vorster M. Concrete bridge protection, repair, and rehabilitation relative to reinforcement corrosion: a methods application manual. Washington (DC): Strategie Highway Research Council SHRP-S-3 60 – National Research Council; 1993.
[2] National Cooperative Highway Research Program. NCHRP Synthesis 333, Transportation Research Board, Washington D.C.; 2004.
[3] Deitz D, Harik I, Gesund H. GFRP reinforced concrete bridge decks, Report KTC-00-9. Lexington, Kentucky: University of Kentucky; 2000.
[4] Mashima M, Iwamoto K. Bond characteristics of FRP rod and concrete after freezing and thawing deterioration. in ACI SP138; 1993. p. 51–70.
[5] Cusson R, Xi Y. The behavior of fiber-reinforced polymer reinforcement in low temperature environmental climates. University of Colorado; 2002.
[6] Karbhari VM, Chin JW, Hunston D, Benmokrane B, Juska T, Morgan R, et al. Durability gap analysis for fiber-reinforced polymer composites in civil infrastructure. ASCE J Compos Construct 2003;7:238–47.
[7] Carvelli V, Pisani MA, Poggi C. Fatigue behaviour of concrete bridge deck slabs reinforced with GFRP bars. Composites: Part B 2010;41:560–7.
[8] El-Ragaby A, El-Salakawy E, Benmokrane B. Fatigue analysis of concrete bridge deck slabs reinforced with E-glass/vinyl ester FRP reinforcing bars. Composites: Part B 2007;38:703–11.
[9] Mufti AA, Neale KW. State-of-the-art of FRP and SHM applications in bridge structures in Canada. Compos Res J 2008;2:60–9.
[10] Pendhari SS, Kant T, Desai YM. Application of polymer composites in civil construction: a general review. Compos Struct 2008;84:114–24.
[11] Nanni A. North American design guidelines for concrete reinforcement and strengthening using FRP: principles, applications and unresolved issues. Construct Build Mater 2003;17:439–46.
[12] Priestley MJN. The thermal response of concrete bridges, in concrete bridges engineering: performance and advances. London: Elsevier Applied Science; 1987. p. 143–188.
[13] CEN EN 1991-1-5: 2003. Eurocode 1 – actions on structures – part 1–5: general actions – thermal actions. Brussels, Belgium: European committee for standardization; 2003.
[14] Sadek AW, El-Hawary MM, El-Dieb AS. Fire resistance testing of concrete beams reinforced by GFRP rebars. J Appl Fire Sci 2006;14:91–104.
[15] Sadek AW, El-Hawary MM, El-Dieb AS. Fire resistance testing of concrete slabs reinforced by GFRP rebars. J Appl Fire Sci 2007;15:131–45.
[16] Nigro E, Cefarelli G, Bilotta A, Manfredi G, Cosenza E. Fire resistance of concrete slabs reinforced with FRP bars. Part I: experimental investigations on the mechanical behavior. Compos Part B: Eng 2011;42:1739–50.
[17] Nigro E, Cefarelli G, Bilotta A, Manfredi G, Cosenza E. Fire resistance of concrete slabs reinforced with FRP bars. Part II: experimental results and numerical simulations on the thermal field. Compos Part B: Eng 2011;42:1751–63.
[18] Di Luzio G, Muciaccia G, Biolzi L. Size effect in thermally damaged concrete. Int J Damage Mech 2010;19:631–56.
[19] Di Luzio G, Biolzi L. Assessing the residual fracture properties of thermally damaged high strength concrete. Mech Mater 2013;4:27–43.
[20] Fire Dynamics Simulator. <https://code.google.com/p/fds-smv/>.
[21] Carvelli V, Pisani MA, Poggi C. High temperature effects on concrete members reinforced with GFRP rebars. Composites: Part B 2013;54:125–32.
[22] CEN EN 1991-2: 2005. Eurocode 1 – actions on structures – Part 2: traffic loads on bridges. Brussels, Belgium; 2005.
[23] CEN EN 1992-2: 2006. Eurocode 2 – design of concrete structures – part 2: concrete bridges. Design and detailing rules. Brussels, Belgium; 2006.
[24] CEN EN 1992-1-1: 2005. Eurocode 2 – design of concrete structures – part 1–1: general rules and rules for buildings. Brussels, Belgium; 2005.
[25] Carvelli V, Fava G, Pisani MA. Anchor system for tension testing of large diameter GFRP bars. ASCE J Compos Construct 2009;13:344–9.
[26] Palmieri A, Matthys S, Taerwe L. Experimental investigation on fire endurance of insulated concrete beams strengthened with near surface mounted FRP bar reinforcement. Composites Part B 2012;43(3):885–95.
[27] Nigro E, Cefarelli G, Bilotta A, Manfredi G, Cosenza E. Guidelines for flexural resistance of FRP reinforced concrete slabs and beams in fire. Composites: Part B 2014;58:103–12.
[28] CEN EN 1992-1-2: 2005. Eurocode 2: design of concrete structures – part 1–2: general rules – structural fire design. Brussels, Belgium; 2005.
[29] Kodur V, Baingo D. Fire resistance of FRP reinforced concrete slabs. National Research Council Canada, Report No. 758; 1998.
[30] Bisby LA, Kodur VKR. Evaluating the fire endurance of concrete slabs reinforced with FRP bars: considerations for a holistic approach. Composites: Part B 2007;38:547–58.

[31] Yu B, Kodur VKR. Factors governing the fire response of concrete beams reinforced with FRP rebars. Compos Struct 2013;100:257–69.
[32] Sargin M. Stress–strain relationships for concrete and the analysis of structural concrete sections. Solid Mechanics Division, University of Waterloo; 1971.
[33] Carreira Domingo J, Chu KH. Stress–strain relationship for plain concrete in compression. ACI J 1986;83:21–8.
[34] Stabler J. Computational modelling of thermomechanical damage and plasticity in concrete – Phd thesis, The University of Qeensland; 2000.
[35] ABAQUS/Standard. Theory and users manuals, release 6.10-1. Pawtucket, RI, USA: HKS Inc.; 2007.
[36] Lubliner J, Oliver J, Oller S, Oñate E. A plastic-damage model for concrete. Int J Solids Struct 1989;25:299–326.
[37] Lee J, Fenves GL. Plastic-damage model for cyclic loading of concrete structures. J Eng Mech 1998;124:892–900.
[38] Nigro E, Bilotta A, Cefarelli G, Manfredi G, Cosenza E. Performance under fire situations of concrete members reinforced with FRP rods: bond models and design nomograms. J Compos Construct – ASCE 2012;16:395–406.
[39] Mufti A, Memon A, Klowak C. Smart steel free bridge decks. In: International workshop on innovative bridge deck technologies, Winnipeg; 2005.
[40] Hassan A, Kawakami M, Niitani k, Yoshioka T. An experimental investigation of steel-free deck slabs. Can J Civ Eng 2002;29(6):831–41.